Alignment of the ALICE MUON spectrometer

J. Castillo[a]
for the ALICE Collaboration

[a]CEA/Dapnia/SPhN
Saclay, France

Abstract

The MUON spectrometer is one of the main detectors of the ALICE experiment at the LHC. The physics programme for the MUON spectrometer will be briefly described. Simulations of the expected performances of the MUON spectrometer in various physics channels with respect to the spectrometer alignment resolution will be discussed. We will then discuss the chosen strategy for the alignment of the MUON spectrometer. Finally, the current performance of the alignment program will be presented.

14.1   Introduction

In ultra-relativistic heavy-ion collisions, our aim is to investigate the properties of nuclear matter under extreme conditions of temperature and pressure which should lead to the creation of deconfined partonic matter, the Quark Gluon Plasma (QGP). With the objective of studying the QGP, heavy-ion collisions were studied at the CERN SPS up to a centre of mass energy $\sqrt{s_{NN}}$ = 17.2 GeV and are currently under investigation at RHIC at BNL with an energy up to $\sqrt{s_{NN}}$ = 200 GeV. The Large Hadron Collider (LHC) at CERN, which is expected to start running during the autumn of 2007, will collide Pb to Pb ions at $\sqrt{s_{NN}}$ = 5.5 TeV providing so far unachieved conditions for studying the QGP.

ALICE is one of the four experiments at the LHC and is the only one that is specifically designed for the high multiplicity environment of heavy-ion collisions. It is composed of various detection systems amongst which is the forward MUON spectrometer. In the next section we shall review the design of the ALICE forward MUON spectrometer, and then briefly review the physics programme of the spectrometer. We shall discuss the expected performances of the spectrometer on a few key physics observables in terms of spectrometer alignment resolution. Afterwards we shall present the chosen strategy for the alignment of the ALICE forward MUON spectrometer and finally discuss the current performance of the alignment software.

14.2   The ALICE forward MUON spectrometer

The forward MUON spectrometer is one of the main detectors of the ALICE experiment and was designed to measure and identify muons at large rapidities. A schematic view of the spectrometer is shown in Fig. 14.1. It consists of

- a front absorber to stop most hadrons, electrons, and photons coming from the interaction point,
- an inner beam shield to stop re-scattered particles from the beam pipe,
- 10 tracking planes to allow particle trajectory reconstruction,
- a large area dipole magnet for momentum determination from track bending,
- a passive muon filter wall followed by four trigger planes that will provide single-muon and muon-pair triggers.

The ALICE forward MUON spectrometer covers an acceptance region from -2.5 to -4.0 in pseudo-rapidity (η) and has full azimuthal coverage. A minimum cut on the transverse momentum ($p_\perp$) of single muons larger than 1.0 GeV/c is applied mainly for background rejection.
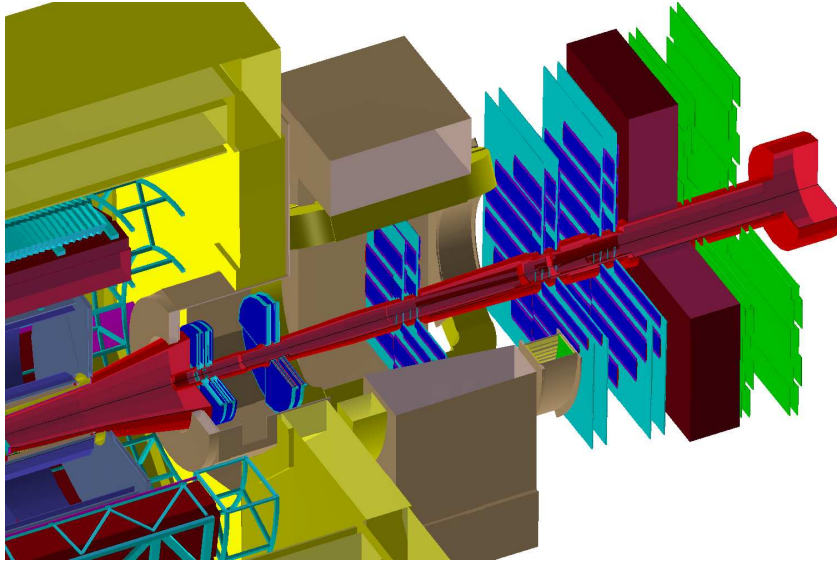
Fig. 14.1: View of the ALICE forward MUON spectrometer.

14.2.1 Tracking system

The tracking system of the ALICE forward MUON spectrometer consists of 10 cathode pad chambers grouped in five stations. Each chamber has two cathode planes in order to provide two-dimensional hit information in the plane transverse to the beam direction, along the track bending direction (vertical axis y) and along the non-bending direction (horizontal axis x). The third dimension is provided by the longitudinal (z) position of the chamber (Section 14.5.1.1 describes the ALICE coordinate system).
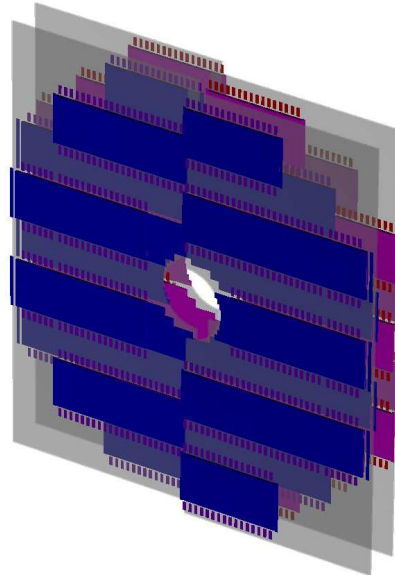
Fig. 14.3: View of station 3
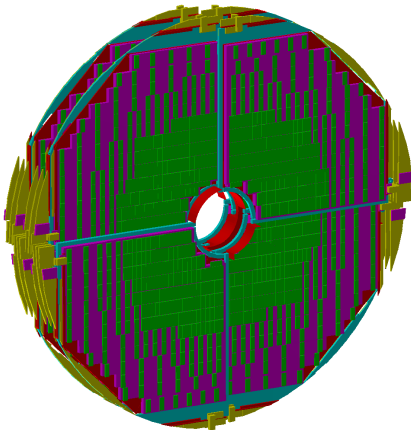
Fig. 14.2: View of station 1

Stations 1 and 2 are located between the front absorber and the dipole magnet. Each chamber of stations 1 and 2 consists of four independents quadrants (see Fig. 14.2). The four quadrants of each chamber are mounted into two independent support structures (aluminium frames) thus defining two independent half chambers at each side of the beam axis along the non-bending direction (x). The quadrants of stations 1 and 2 add-up to a total of 16 independent detection elements.

Station 3 is located inside the dipole magnet and plays a crucial role in determining the track bending. In

view of the large surface covered by station 3 a modular design based on a *slat* geometry is therefore used (see Fig. 14.3). Each chamber consists of 18 independent slats. The 18 slats of each chamber are also mounted into two independent support structures (carbon/epoxy fibre panels). Station 3 consists of a total of 36 detection elements.

Finally, stations 4 and 5 are located between the dipole magnet and the muon filter wall. A slat geometry is also used for stations 4 and 5 and each chamber consists of 26 independent slats mounted into two half chambers as for station 3. A total of 104 detection elements compose stations 4 and 5.

Therefore, the tracking system of the ALICE forward MUON spectrometer consists of 156 independent detection elements, each providing two-dimensional hit positions. All detection elements were designed to provide a combined spatial resolution of 100 μm for the bending coordinate and 1 mm for the non-bending coordinate.

More detailed information on the ALICE forward MUON spectrometer design can be found in its technical design report [1, 2].

14.2.2 Degrees of freedom and initial misalignment

Each one of the 156 detection elements has, in principle, six degrees of freedom, three translations and three rotations. The expected initial resolution and the relevance of these six parameters will be discussed later. Also, since the detection elements are mounted into independent support structures, six further degrees of freedom per half-chamber should be considered.

The initial position of the half-chambers will be measured by the CERN survey group with 1 mm resolution in the three directions. The displacements of the half-chambers relative to a reference chamber will be periodically monitored by the Geometrical Monitoring System (GMS) with $\sim$ 20 μm resolution in the three directions. The absolute positioning of the reference chamber will be monitored with $\sim$ 500 μm. However, this global displacement will only have a minor impact on the physics capabilities of the spectrometer [3, 4].

The mechanical precision of the attach points of the detection elements into their respective support structures is $\sim$ 500 μm in all cases. A survey by a photogrammetry method will provide the initial position of the detection elements with respect to their support structure with an expected resolution of 100 μm along the beam axis and 50 μm in the two directions perpendicular to the beam axis. However, the photogrammetry method will only be performed once before the start-up of the LHC. Alignment with tracks will be needed to trace any further misalignment. For example, the one expected from the thermal expansion of the support structures due to heating from the electronics.

14.3 Physics programme of the ALICE forward MUON spectrometer

One of the main objectives of the ALICE experiment is to study the properties of nuclear matter under extreme conditions of temperature and pressure produced in ultra-relativistic heavy-ion collisions at the LHC. It is expected that deconfined partonic matter, the QGP, will be created.

Whilst several observables have been proposed to characterize the QGP, the study of heavy quark c and b production is thought to be one of the most powerful probes. The forward MUON spectrometer is specially designed to study heavy quark production in heavy-ion collisions at the LHC.

A detailed description of the physics programme of the ALICE forward MUON spectrometer can be found in Chapters 6.6 and 6.7 of the ALICE Physics Performance Report, Volume II [5]. We will give a brief review of this programme below.

14.3.1 Quarkonia production

The study of the production of heavy quark and antiquark bound states (quarkonia), J/Ψ, Ψ' ($c\bar{c}$), Υ(1S), Υ(2S) and Υ(3S) ($b\bar{b}$) is among the priorities for the ALICE forward MUON spectrometer and will be done by the analysis of the invariant mass distribution of opposite-sign muon pairs. It was first proposed that quarkonia resonances will sequentially dissociate by colour screening in the presence of a QGP [6], thus a suppression of quarkonia production in ion–ion collisions compared with proton–ion collisions was predicted as a signature for QGP formation. Later, it was also proposed that additional quarkonia production mechanisms, such as quark recombination in the QGP [7], could add up to the prompt production by initial hard scattering. In this case an enhanced production of quarkonia resonances will be observed in ion–ion collisions. The recombination scenarios are expected to be important for the charmonium states at RHIC energies and even more at LHC energies.

The current results at lower energies, at the SPS and RHIC, have so far been inconclusive and even puzzling. The results from the LHC will allow us to differentiate between the different quarkonia production scenarios. The ALICE forward MUON spectrometer must then be able to measure clearly the above-mentioned quarkonia resonances and, in particular, it should be able to separate the three $b\bar{b}$ states. This requires a maximum invariant mass resolution of 100 MeV/c^2 at the mass of the Υ.

14.3.2 Open charm and beauty production

Open charm (D mesons) and open beauty (B mesons) production studies are also among the priorities for the

ALICE forward MUON spectrometer. On the one hand, they are interesting on their own as they will allow us to extract the charm and beauty cross-sections and thus apply further constraints on perturbative QCD calculations. On the other hand, open charm and open beauty measurements could be used as a reference for the quarkonia studies in ion–ion collisions.

Open charm and open beauty production will be measured in the ALICE forward MUON spectrometer via their muonic decay channels. The first measurement of open charm and open beauty will probably be extracted from the single muon $p_\perp$ distributions. Decay muons from π and K will dominate at low transverse momentum, while D and B contributions should dominate at $p_\perp$ larger than 5–8 GeV/c.

Like- and unlike-sign muon pairs originating from the same hard scattering or same heavy quark, will present a residual correlation in the low (1–3 GeV/c^2) and high (4–8 GeV/c^2) invariant mass regions. Correlated unlike-sign muon pairs in the higher invariant mass region will mainly be produced by semi-muonic decays of D–$\bar{D}$ and B–$\bar{B}$ mesons from the same hard scattering. The lower invariant mass region will be primarily populated by the B–D ($\bar{B}$–$\bar{D}$) semi-muonic decay chain from the same b ($\bar{b}$) quark fragmentation.

14.3.3 Other projected analysis

The physics programme is continuously becoming enriched with perhaps more challenging analysis. Among the latest proposals we can mention the analysis of the polarization of the J/Ψ which will need a clean reconstruction of the J/Ψ peak and good angular resolution. Also, the measurement of electroweak bosons (W and Z) should be possible through their muonic decay. Muons from W and Z bosons decays should dominate the single muon transverse momentum distribution for $p_\perp$ larger than ~ 30 GeV/c [8]. Finally, the study of three muon correlations should give access to the $b - \bar{b}$ production cross-section as well as provide information on feed-down of J/Ψ from B mesons decays.

14.4 Expected physics performances of the ALICE forward MUON spectrometer

In Section 14.3 we mentioned that the J/Ψ and Υ resonances are among the key physics observables of the ALICE forward MUON spectrometer. It is thus essential to understand how the measurement of the J/Ψ and Υ resonances is affected by the misalignment of the spectrometer.

14.4.1 Geometry and misalignment definitions

In AliRoot the position of each tracking chamber of the ALICE forward MUON spectrometer is defined by the position of its centre and by the three rotation angles

around the three axes. In addition, each independent detection element (slat or quadrant) is defined relative to the tracking chamber it belongs to by the position of the centre and the three rotation angles.

The misalignments of the spectrometer are defined by small deltas of any of the above-mentioned positions or rotations with respect to an ideal geometry. More details on the common approach in ALICE to define and apply these misalignments can be found in Ref. [9].

Table 14.1: Gaussian widths of misalignment distributions

|	$\sigma_x(\mu m)$	$\sigma_y(\mu m)$	$\sigma_\phi(\mu rad)$
Set 00	0	0	0
Set 005	50	50	87
Set 01	100	100	175
Set 03	300	300	523
Set 05	500	500	872
Set 07	700	700	1222
Set 10	1000	1000	1745

14.4.2 Misalignment simulations

For the following study we will consider only independent random translations of the detection elements along the x and y axis and random rotations about the z axis (azimuthal angle). To the first order these three transformations are the most relevant for tracking throughout the spectrometer. However, the effect of the other three transformations should be studied.

We generated misalignment files where the independent transformation parameters were taken from gaussian distributions centred at 0 and with a width σ given in Table 14.1. These files were stored in a local Calibration Data Base (CDB) [9].
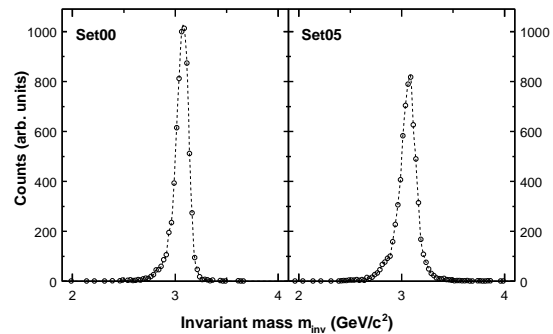
Fig. 14.4: J/Ψ invariant mass distribution for the misalignment sets: Set 00 (left panel) and Set 05 (right panel)
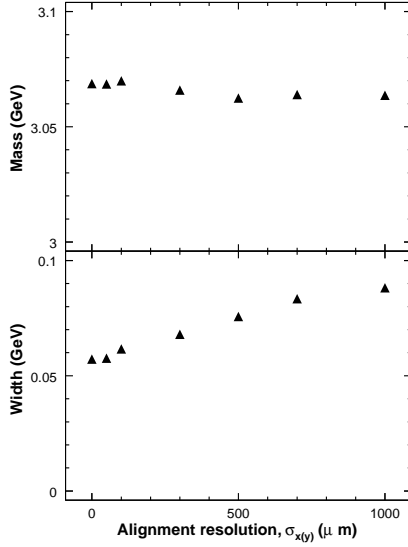
Fig. 14.5: Mass (top) and width (bottom) of the J/Ψ as a function of the alignment resolution $\sigma_{x(y)}$

### 14.4.3 J/Ψ and Υ invariant mass distributions

For each misalignment set in Table 14.1 we simulated, independently, 10 000 J/Ψ and 10 000 Υ in the acceptance of the ALICE forward MUON spectrometer using a realistic $p_{\perp}$ and y distribution and the decays were forced into the $\mu^{+}\mu m$ channel. The μ were propagated through the detector using GEANT3. The full reconstruction code of the ALICE forward MUON spectrometer was then used to reconstruct the simulated events. The simulation step was performed using the ideal geometry whilst the reconstruction step was repeated using each set of misalignments.

Figure 14.4 shows the resulting J/Ψ invariant mass distribution for the misalignment sets Set 00 (left panel) and Set 05 (right panel). A deterioration of the invariant mass peak of the J/Ψ is clearly visible. The effect of the misalignment on the J/Ψ peak can be quantified by fitting the peak to a Gaussian distribution centred at *mass* and with a sigma *width*. We restrict the fit to $[\text{mass} - 2 \cdot \text{width}; \text{mass} + 2 \cdot \text{width}]$ to avoid the non-Gaussian tail in the invariant mass distribution due to the absorber. Figure 14.5 shows the mass (top) and width (bottom) of the J/Ψ obtained as a function of $\sigma_{x(y)}$. On the one hand, we do not observe any significant variation of the J/Ψ mass through the range of misalignment studied. On the other hand, we do observe a clear increase on the J/Ψ invariant mass resolution for misalignments characterized by $\sigma_{x(y)} \geq 100 \ \mu m$. To avoid deteriorating the J/Ψ invariant mass resolution by more than $\sim 10\%$ we must restrain the misalignments of the detection elements to $\sigma_{x(y)} \leq 100 \ \mu m$.
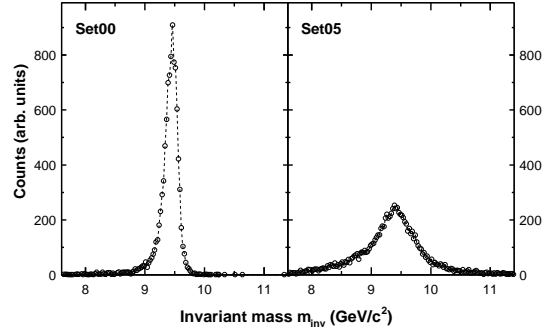
Fig. 14.6: Υ invariant mass distribution for the misalignment sets: Set 00 (left panel) and Set 05 (right panel)

Figure 14.6 shows the Υ invariant mass distribution for the misalignment sets; Set 00 (top panel) and Set 05 (bottom panel). The deterioration of the Υ peak with misalignment is clearly visible and the effect is stronger than for the J/Ψ. We can also note that the non-Gaussian tail at low invariant mass is more prominent for the Υ, thus for the Υ we restrict the fit to $[\text{mass} - 1.5 \cdot \text{width}; \text{mass} + 1.5 \cdot \text{width}]$. Figure 14.7 shows the mass (top) and width (bottom) of the Υ obtained as a function of $\sigma_{x(y)}$. In the case of the Υ we note a drop in the reconstructed mass with increasing misalignment. Moreover, we observe a stronger increase in the invariant mass resolution for the Υ than that for the J/Ψ. For the Υ we should restrain the misalignment to $\sigma_{x(y)} \leq 50 \ \mu m$ to keep the increase of the invariant mass resolution smaller than $\sim 10\%$.
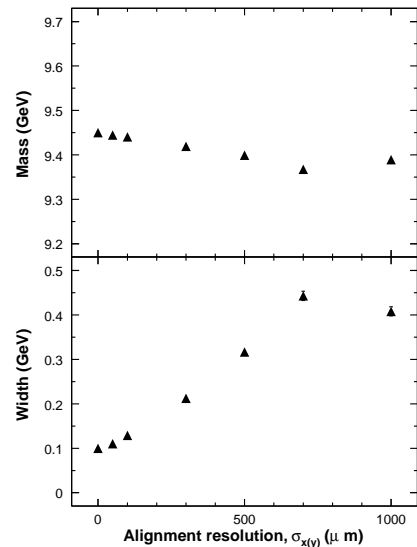
Fig. 14.7: Mass (top) and width (bottom) of the Υ as a function of the alignment resolution $\sigma_{x(y)}$

We note that the J/Ψ (Υ) reconstruction efficiency is constant in all cases except for the misalignment set Set 10 for which we observe a 15% drop. We also note that the above results for the Υ are consistent with the results from earlier simulations [10]. However, those simulations were done using a now obsolete geometry of the MUON spectrometer. It was therefore important to update the simulations using an updated geometry and simulation, and reconstruction software, as well as to extend them to the J/Ψ.

We have seen that a proper reconstruction of the Υ constitutes the limiting case for an acceptable misalignment. Thus, we must be able to align the detection element with a maximum resolution of $\sigma_{x(y)} = 50 \ \mu$m and $\sigma_\phi = 87 \ \mu$rad. This determines the minimum performance that the alignment program must provide.

14.5 Alignment strategy

The alignment of tracking detectors usually requires the determination of a large number of alignment parameters (at least 468 for the ALICE forward MUON spectrometer). Usually special alignment data (like geometrical surveys) are used together with reconstructed tracks from physics data in order to determine the alignment parameters.

To obtain the alignment parameters from reconstructed tracks an approximate method is typically used: the mean *residual* distance between the reconstructed track extrapolation and the measured track impact (hit) is used to correct the alignment parameters of the current detection element. This is equivalent to a least square minimization with respect to the alignment parameters. However, this approximate method is not statistically correct, as discussed in Refs. [11, 12], as it is biased by the ignorance of the alignment parameters when initially reconstructing the tracks. While an iterative approach to this method is often used to reduce the residuals the alignment parameters will remain biased.

An optimal method will be to perform a least square minimization with respect to the alignment and the track parameters simultaneously. This method is, however, limited practically by the calculation time necessary to perform the minimization with respect to the large amount of parameters involved. A special method was developed by V. Blobel [11] to deal with the particular case of an alignment problem. Indeed, in a detector alignment problem we can differentiate two types of parameters, those that apply to all the measurements (alignment parameters), and those that apply to a single measurement (track parameters). This special structure allows one to extract an exact solution with a greatly reduced calculation time. The FORTRAN program Millepede [13] implements this method. More details about Millepede can also be found in V. Blobel's contribution to this report [12].

We have thus chosen to use the Millepede method for the alignment of the ALICE forward MUON spectrometer using physics tracks. It is worth noting that Millepede has been successfully applied to other experiments like COMPASS at CERN or PHENIX at RHIC.
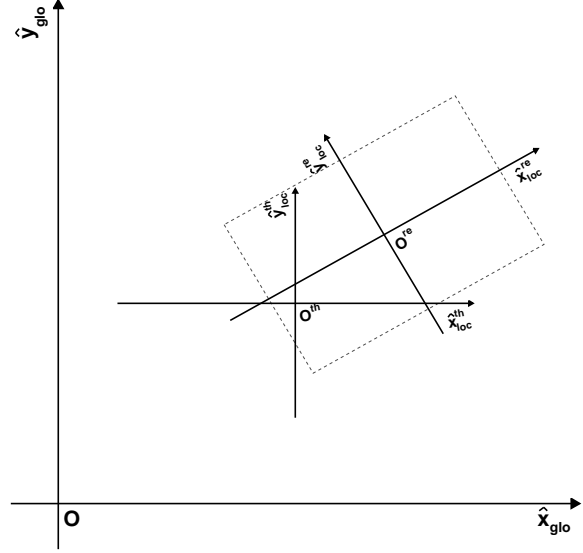
Fig. 14.8: Theoretical (O^{th}, $\hat{x}_{\text{loc}}^{\text{th}}$, $\hat{y}_{\text{loc}}^{\text{th}}$, $\hat{z}_{\text{loc}}^{\text{th}}$) and real ($O^{\text{re}}$, $\hat{x}_{\text{loc}}^{\text{re}}$, $\hat{y}_{\text{loc}}^{\text{re}}$, $\hat{z}_{\text{loc}}^{\text{re}}$) local reference frames of a given detection element of the ALICE forward MUON spectrometer. The global ALICE coordinate system (O, $\hat{x}_{\text{glo}}$, $\hat{y}_{\text{glo}}$, $\hat{z}_{\text{glo}}$ is also shown. In all cases $\hat{z}$ goes out of the board.

14.5.1 Application of Millepede to the MUON spectrometer alignment

14.5.1.1 Coordinate systems and alignment parameters

The ALICE coordinate system is described in detail elsewhere [14]. It is a right-handed orthogonal Cartesian system with point of origin (O) x, y, z = 0 at the nominal interaction point (IP). The x axis is perpendicular to the mean beam axis, parallel to the local horizon, and pointing towards the centre of the LHC rings. The y axis is also perpendicular to the mean beam axis and is pointing upwards. Finally, the z axis is parallel to the mean beam axis. The ALICE forward MUON spectrometer is located at negative z.

The theoretical (O^{th}, $\hat{x}_{\text{loc}}^{\text{th}}$, $\hat{y}_{\text{loc}}^{\text{th}}$, $\hat{z}_{\text{loc}}^{\text{th}}$) and real ($O^{\text{re}}$, $\hat{x}_{\text{loc}}^{\text{re}}$, $\hat{y}_{\text{loc}}^{\text{re}}$, $\hat{z}_{\text{loc}}^{\text{re}}$) local frames of a given detection element of the ALICE forward MUON spectrometer are depicted in Fig. 14.8 with respect to the global ALICE coordinate system (O, $\hat{x}_{\text{glo}}$, $\hat{y}_{\text{glo}}$, $\hat{z}_{\text{glo}}$). We can then define the detection elements misalignment as the transformation from (O^{th}, $\hat{x}_{\text{loc}}^{\text{th}}$, $\hat{y}_{\text{loc}}^{\text{th}}$, $\hat{z}_{\text{loc}}^{\text{th}}$) to ($O^{\text{re}}$, $\hat{x}_{\text{loc}}^{\text{re}}$, $\hat{y}_{\text{loc}}^{\text{re}}$, $\hat{z}_{\text{loc}}^{\text{re}}$), which can be decomposed into three translations

of O^{re} along $\hat{x}_{\mathrm{glo}}$, $\hat{y}_{\mathrm{glo}}$ and $\hat{z}_{\mathrm{glo}}$ and the three rotations around $\hat{x}_{\mathrm{glo}}$, $\hat{y}_{\mathrm{glo}}$ and $\hat{z}_{\mathrm{glo}}$.

For the current study we shall, however, only consider the two translations along $\hat{x}_{\mathrm{glo}}$, $\hat{y}_{\mathrm{glo}}$ and the rotation around $\hat{z}_{\mathrm{glo}}$ (azimuthal rotation). Therefore, for each detection element we will consider three alignment (global) parameters: $\delta_x = x^{\mathrm{re}}_{\mathrm{loc}} - x^{\mathrm{th}}_{\mathrm{loc}}$, $\delta_y = y^{\mathrm{re}}_{\mathrm{loc}} - y^{\mathrm{th}}_{\mathrm{loc}}$ and $\delta_\phi = \phi^{\mathrm{re}}_{\mathrm{loc}} - \phi^{\mathrm{th}}_{\mathrm{loc}}$.

14.5.1.2 Magnetic field and track parameters

The next step after defining the alignment parameters is to define the track model that describes the path of a particle flying through the detector and thus the track parameters.

In the case without a magnetic field the track of a particle is a simple straight line. The crossing point (x_j, y_j) of a particle at the detection element at the plane located at $z = z_j$ is then given by

$$\left\{ \begin{array}{l} x_j = x_0 + t_x(z_j - z_0) \\ y_j = y_0 + t_y(z_j - z_0) \end{array} \right. \qquad (14.1)$$

where (x_0, y_0) is the track position at a reference plane at $z = z_0$, and t_x and t_y are the slope parameters in the $(\hat{x}_{\mathrm{glo}}, \hat{z}_{\mathrm{glo}})$ and $(\hat{y}_{\mathrm{glo}}, \hat{z}_{\mathrm{glo}})$ planes, respectively. x_0, y_0, t_x and t_y are the track (local) parameters.

The case with a non-zero magnetic field is more complex since the track of a particle is no longer a simple straight line. In the ALICE forward MUON spectrometer we use a Kalman tracker and fitter. For the alignment program we could consider a linear approximation to the tracks (for high enough transverse momentum) or a local straight track approximation at each measured point. Studies are currently ongoing in this direction but are so far inconclusive.

14.5.1.3 Linear expression of residuals

As discussed in section 14.5 the optimal approach to determine the alignment parameters is to minimize the residuals with respect to the alignment and the track parameters simultaneously. The χ^2 to minimize can be written as

$$\chi^2 = \sum_{i=1}^{N_{\mathrm{tracks}}} \chi_i^2, \qquad (14.2)$$

where the χ_i^2 of track i is given by

$$\chi_i^2 = \sum_{j=1}^{N_{\mathrm{det}}} \frac{F_{i,j}\left(x^{\mathrm{m}}_{\mathrm{loc}}, y^{\mathrm{m}}_{\mathrm{loc}}, \mathrm{par}_{\mathrm{align}}, \mathrm{par}^i_{\mathrm{track}}\right)^2}{\sigma_j^2}. \qquad (14.3)$$

$F_{i,j}$ is the residual of track i at the detection element j which is a function of the measured local coordinates of the track hit in the detection element j, $x^{\mathrm{m}}_{\mathrm{loc}}$ and $y^{\mathrm{m}}_{\mathrm{loc}}$, of the set of alignment parameters $\mathrm{par}_{\mathrm{align}}$ and of the track parameters of track i $\mathrm{par}^i_{\mathrm{track}}$. σ_j^2 is the intrinsic resolution of the detection element j.

In order to use Millepede to obtain the alignment parameters we need to derive a linear expression of the track residuals $F_{i,j}$. By definition $F_{i,j}$ is the distance between the extrapolation of track i to the detection element j ($x^{\mathrm{tr}}_{\mathrm{loc}}$, $y^{\mathrm{tr}}_{\mathrm{loc}}$, $z^{\mathrm{tr}}_{\mathrm{loc}}$) and the measured position of the track hit by the detection element j ($x^{\mathrm{m}}_{\mathrm{loc}}$, $y^{\mathrm{m}}_{\mathrm{loc}}$, $z^{\mathrm{m}}_{\mathrm{loc}}$) in the detection element local coordinates. $F_{i,j}$ is thus given by:

$$F_{i,j} = \left\{ \begin{array}{l} x^{\mathrm{tr}}_{\mathrm{loc}} - x^{\mathrm{m}}_{\mathrm{loc}} \\ y^{\mathrm{tr}}_{\mathrm{loc}} - y^{\mathrm{m}}_{\mathrm{loc}} \\ z^{\mathrm{tr}}_{\mathrm{loc}} - z^{\mathrm{m}}_{\mathrm{loc}} \end{array} \right. . \qquad (14.4)$$

Since we will not consider any possible misalignment along $\hat{z}_{\mathrm{glo}}$, then $z^{\mathrm{tr}}_{\mathrm{loc}} = z^{\mathrm{m}}_{\mathrm{loc}}$. The expression of $F_{i,j}$ reduces to:

$$F_{i,j} = \left\{ \begin{array}{l} x^{\mathrm{tr}}_{\mathrm{loc}} - x^{\mathrm{m}}_{\mathrm{loc}} \\ y^{\mathrm{tr}}_{\mathrm{loc}} - y^{\mathrm{m}}_{\mathrm{loc}} \end{array} \right. . \qquad (14.5)$$

Figure 14.9 shows that this distance can be obtained by applying a change of reference frame from the global ALICE reference frame to the *real* local (*i.e.* including misalignment) reference frame. Thus, we can write:

$$F_{i,j} = \left\{ \begin{array}{l} \left\{\cos(\phi + \delta\phi)\left[x^{\mathrm{tr}} - (x^{O^{\mathrm{th}}} + \delta_x)\right] + \sin(\phi + \delta\phi)\left[y^{\mathrm{tr}} - (y^{O^{\mathrm{th}}} + \delta_y)\right]\right\} - x^{\mathrm{m}}_{\mathrm{loc}} \\ \left\{-\sin(\phi + \delta\phi)\left[x^{\mathrm{tr}} - (x^{O^{\mathrm{th}}} + \delta_x)\right] + \cos(\phi + \delta\phi)\left[y^{\mathrm{tr}} - (y^{O^{\mathrm{th}}} + \delta_y)\right]\right\} - y^{\mathrm{m}}_{\mathrm{loc}} \end{array} \right. . \qquad (14.6)$$

The alignment parameters δ_x, δ_y and δ_ϕ are supposed to be *small* corrections to an ideal position of the detection elements. We can then derive a linear expression of $F_{i,j}$ by an expansion to the first order in δ_x, δ_y and δ_ϕ:

$$F_{i,j} = \left\{ \begin{array}{l} \cos(\phi)\left[x^{\mathrm{tr}} - x^{O^{\mathrm{th}}}\right] + \sin(\phi)\left[y^{\mathrm{tr}} - y^{O^{\mathrm{th}}}\right] \\ -\cos(\phi)\delta_x - \sin(\phi)\delta_y + \left[-\sin(\phi)\left[x^{\mathrm{tr}} - x^{O^{\mathrm{th}}}\right] + \cos(\phi)\left[y^{\mathrm{tr}} - y^{O^{\mathrm{th}}}\right]\right]\delta_\phi - x^{\mathrm{m}}_{\mathrm{loc}} \\ \\ -\sin(\phi)\left[x^{\mathrm{tr}} - x^{O^{\mathrm{th}}}\right] + \cos(\phi)\left[y^{\mathrm{tr}} - y^{O^{\mathrm{th}}}\right] \\ +\sin(\phi)\delta_x - \cos(\phi)\delta_y + \left[-\cos(\phi)\left[x^{\mathrm{tr}} - x^{O^{\mathrm{th}}}\right] - \sin(\phi)\left[y^{\mathrm{tr}} - y^{O^{\mathrm{th}}}\right]\right]\delta_\phi - y^{\mathrm{m}}_{\mathrm{loc}} \end{array} \right. . \qquad (14.7)$$

The next step is to derive the linear expression of $F_{i,j}$ with respect to the track parameters x_0, y_0, t_x and t_y [see Eq. (14.1)]. We replace x^{tr} and y^{tr} in Eq. (14.7) by their expressions from Eq. (14.1). Also, since δ_ϕ (δ_x,

δ_y) is small and since we will be interested only in the derivatives of $F_{i,j}$ with respect to to the track or alignment parameters, we can neglect the term in δ_ϕ in the derivative terms with respect to the track parameters. Thus, we obtain the linear expression:

$$F_{i,j} = \begin{cases} \cos(\phi)x_0 + \sin(\phi)y_0 + \cos(\phi)\big[z_j - z_0\big]t_x + \sin(\phi)\big[y_j - z_0\big]t_y \\ - \cos(\phi)\delta_x - \sin(\phi)\delta_y + \Big[- \sin(\phi)\big[x^{\mathrm{tr}} - x^{O^{\mathrm{th}}}\big] + \cos(\phi)\big[y^{\mathrm{tr}} - y^{O^{\mathrm{th}}}\big]\Big]\delta_\phi \\ \qquad - \cos(\phi)x^{O^{\mathrm{th}}} - \sin(\phi)y^{O^{\mathrm{th}}} - x_{\mathrm{loc}}^{\mathrm{m}} \\ \\ - \sin(\phi)x_0 + \cos(\phi)y_0 - \sin(\phi)\big[z_j - z_0\big]t_x + \cos(\phi)\big[y_j - z_0\big]t_y \\ + \sin(\phi)\delta_x - \cos(\phi)\delta_y + \Big[- \cos(\phi)\big[x^{\mathrm{tr}} - x^{O^{\mathrm{th}}}\big] - \sin(\phi)\big[y^{\mathrm{tr}} - y^{O^{\mathrm{th}}}\big]\Big]\delta_\phi \\ \qquad + \sin(\phi)x^{O^{\mathrm{th}}} - \cos(\phi)y^{O^{\mathrm{th}}} - x_{\mathrm{loc}}^{\mathrm{m}} \end{cases} . \tag{14.8}$$
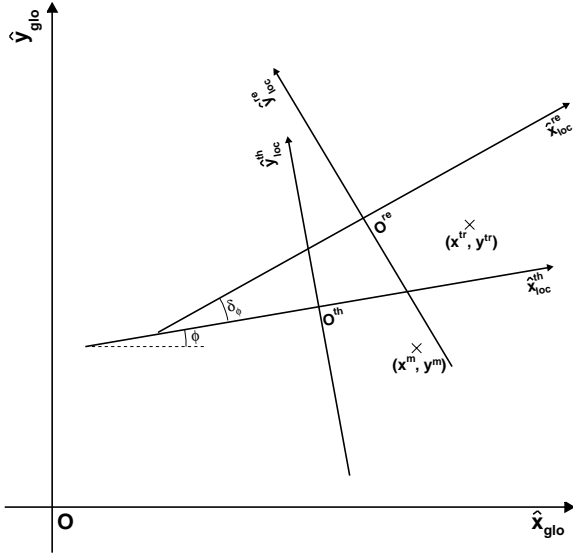
Fig. 14.9: Track extrapolation $(x^{\mathrm{tr}}, y^{\mathrm{tr}})$ and measured hit position $(x^{\mathrm{tr}}, y^{\mathrm{tr}})$ to and by a given detection element. The theoretical $(O^{\mathrm{th}}, \hat{x}_{\mathrm{loc}}^{\mathrm{th}}, \hat{y}_{\mathrm{loc}}^{\mathrm{th}}, \hat{z}_{\mathrm{loc}}^{\mathrm{th}})$ and real $(O^{\mathrm{re}}, \hat{x}_{\mathrm{loc}}^{\mathrm{re}}, \hat{y}_{\mathrm{loc}}^{\mathrm{re}}, \hat{z}_{\mathrm{loc}}^{\mathrm{re}})$ local reference frames are shown. In all cases $\hat{z}$ goes out of the board.

We note that the expression of Eq. (14.8) is further simplified if $\phi = 0$, i.e., if the ideal local reference frame of the detection element is just a translation of the global ALICE frame which is the case of the ALICE forward MUON spectrometer. We also note that in the above case the constant term of $F_{i,j}$ reduce to $(x^{\mathrm{m}}, y^{\mathrm{m}})$, which are the measured hit coordinates in the global reference frame. We shall, however, keep the more general expression for $\phi \neq 0$.

From Eq. (14.8) we can easily extract the residual derivatives with respect to the track and alignment parameters as well as the constant terms to be fed to the Millepede program.

14.5.2 AliMillepede

The original implementation of Millepede by V. Blobel [13] was written in FORTRAN. It is however a policy of the ALICE Off-line Project to use only code written in C++, following a set of defined coding conventions [15], "except for large existing libraries [...] and some remaining legacy code". A C++ version of Millepede, complying with the ALICE Off-line Project coding conventions was therefore needed.

The AliMillepede [16] class is a modified version of a C++ implementation of Millepede by S. Viret [17] for the LHCb experiment. The alignment results using AliMillepede were checked against those obtained using the original FORTRAN version and were found to be fully compatible. AliMillepede was therefore validated and all the alignment results shown here were obtained using it.

14.6 Current performances of the alignment program

As a first test of the alignment of the ALICE forward MUON spectrometer using the Millepede approach we simulated a misalignment of the detection elements following uniform distributions with $-300 < \delta_x(\mu\mathrm{m}) < 300$, $-300 < \delta_y(\mu\mathrm{m}) < 300$, and $-523 < \delta_\phi(\mu\mathrm{rad}) < 523$. The distribution of the input misalignments for the 156 detection elements are shown in Fig. 14.10. For this first study we only considered the misalignment of stations 3, 4 and 5 (slat type) and we fixed the detection elements of stations 1 and 2 to their known positions. With the misalignment generated above we simulated 30 000 events each containing 10 μ's in the MUON spectrometer acceptance. We performed a full simulation applying the misalignments and ran the standard reconstruction using the ideal geometry. The resulting tracks were fed to Millepede.
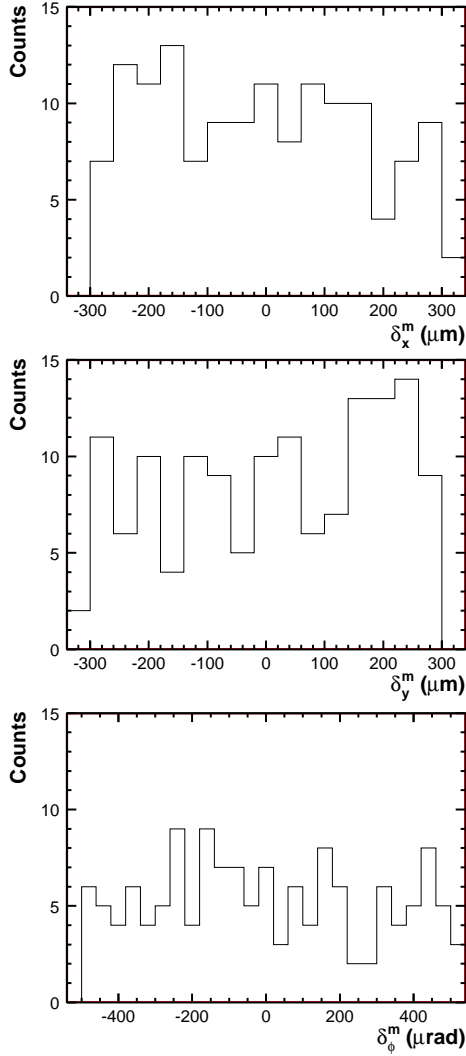
Fig. 14.10: Distribution of the input misalignments δ_x^{m} (top), δ_y^{m} (centre), and δ_ϕ^{m} (bottom)

Figure 14.11 shows the distributions of the difference between the simulated misalignment and the calculated misalignment by the alignment program for δ_x (top), δ_y (centre), and δ_ϕ (bottom). We first observe that the alignment code is able to align the spectrometer and that the alignment resolutions obtained are $\sim 50\,\mu\mathrm{m}$ for δ_x and δ_y, and $\sim 30\,\mu\mathrm{rad}$ for δ_ϕ. However, it is also evident that the distributions of $\delta_x^{\mathrm{m}} - \delta_x^{r}$ and $\delta_y^{\mathrm{m}} - \delta_y^{r}$ show a double peak structure. This is indicative of some correlated displacements of the detection elements which can not be constrained by the alignment program.

The correlated displacements observed can be more clearly seen in Fig. 14.12 (top panel) which compares the simulated misalignment δ_x^{m} (red symbols) to the calculated misalignments δ_x^{r} (black symbols) as a function of the detection element id for chamber 7. The

systematic pattern observed corresponds to a common translation along $\hat{x}_{\mathrm{glo}}$ of the detection elements at $x < 0$ in one direction and of the detection elements at $x > 0$ in the other direction. The same applies to common translations along the $\hat{y}_{\mathrm{glo}}$ for upper and lower detection elements [Fig. 14.12 (bottom panel)]. Indeed, these kind of correlated global displacements cannot be constrained by the alignment code.
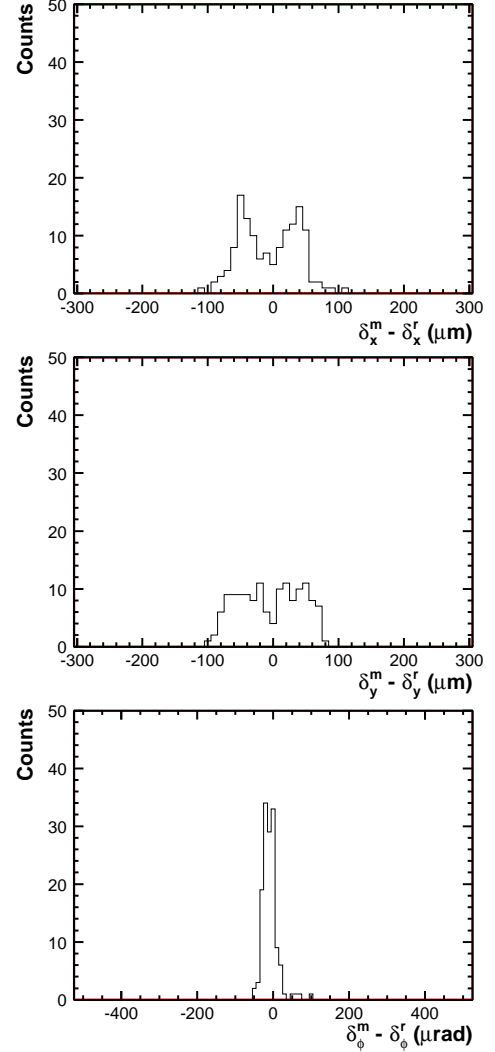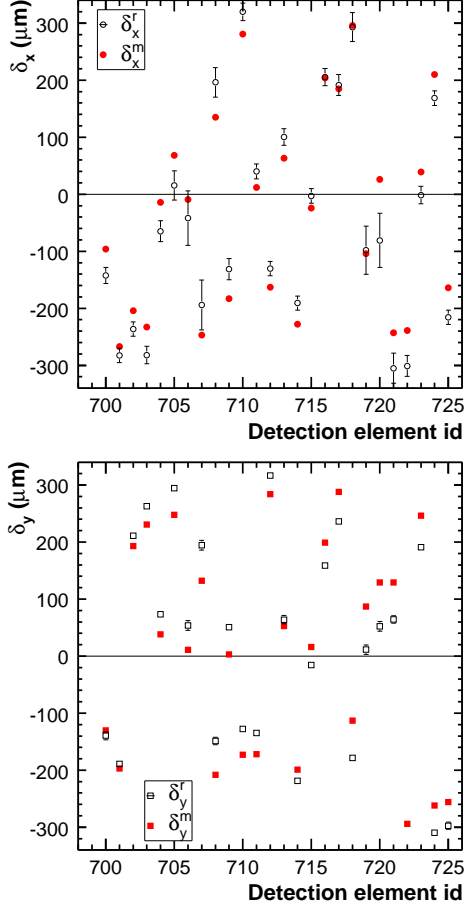

Fig. 14.11: Distributions obtained: $\delta_x^{\mathrm{m}} - \delta_x^{r}$ (top), $\delta_y^{\mathrm{m}} - \delta_y^{r}$ (centre), and $\delta_\phi^{\mathrm{m}} - \delta_\phi^{r}$ (bottom)

14.6.1 Constraining the alignment parameters

We need to apply some kind of constraints on the alignment parameters in order to avoid the correlated movements. In the Millepede program, constraints on the alignment parameters can be easily applied in two ways:

– Fix the allowed variation for a given alignment

135

parameter.
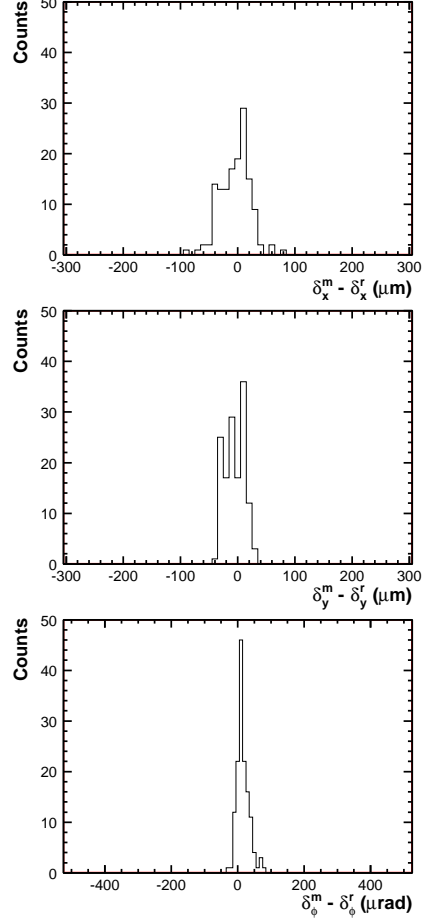– Constrain a linear combination of some alignment parameters.

resolutions are sufficient to carry the foreseen physics programme of the ALICE forward MUON spectrometer as discussed in Sections 14.3 and 14.4.

Fig. 14.12: Top panel: Comparison of the simulated misalignment δ_x^{m} (red closed circles) with the calculated misalignments δ_x^r (black open circles) as a function of the detection element id for chamber 7. Bottom panel: Same between δ_y^{m} (red closed squares) and δ_y^r (black open squares).

Fig. 14.13: $\delta_x^{\mathrm{m}} - \delta_x^r$ (top), $\delta_y^{\mathrm{m}} - \delta_y^r$ (centre), and $\delta_\phi^{\mathrm{m}} - \delta_\phi^r$ (bottom) distributions using global constraints (see text for details)

For instance, the first item could be used to constrain the alignment parameters to their mechanical accuracy. The second item can be used to avoid correlated movements of the detector by the alignment process. We used this mechanism to constrain global translations along $\hat{x}_{\mathrm{glo}}$ and $\hat{y}_{\mathrm{glo}}$ to the above alignment case.

Figure 14.13 shows the distributions of $\delta_x^{\mathrm{m}} - \delta_x^r$ (top), $\delta_y^{\mathrm{m}} - \delta_y^r$ (centre), and $\delta_\phi^{\mathrm{m}} - \delta_\phi^r$ (bottom) obtained when applying the global constraints mentioned. We first observe that the double peak structure has now disappeared. Second, we observe an improved alignment resolution for the three alignment parameters: $\sim 30\ \mu\mathrm{m}$ for δ_x, $\sim 20\ \mu\mathrm{m}$ for δ_y, and $\sim 20\ \mu\mathrm{rad}$ for δ_ϕ. These
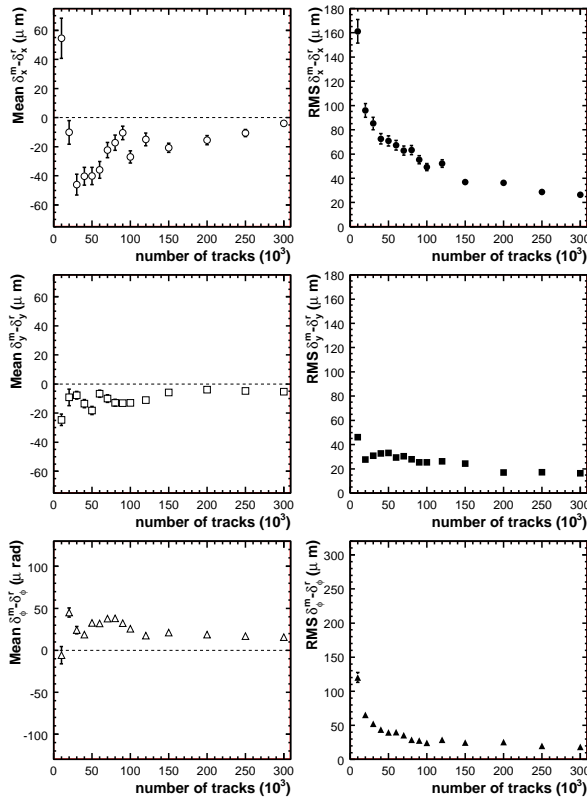
14.6.2 Number of tracks

Figure 14.14 shows the dependence of the mean (left panels) and r.m.s. (right panels) of the $\delta_x^{\mathrm{m}} - \delta_x^r$ (top), $\delta_y^{\mathrm{m}} - \delta_y^r$ (centre) and $\delta_\phi^{\mathrm{m}} - \delta_x^\phi$ (bottom) distributions obtained with the number of tracks (N_{tracks}) used by the alignment program. We observe that the best results are already obtained for $N_{\mathrm{tracks}} \sim 150\,000$ and that a further increase of N_{tracks} does not significantly improve the alignment results.

14.7 Conclusions and outlook

We have studied some of the possible impacts that misalignments of the detection elements of the ALICE forward MUON spectrometer will have on the quarkonia physics programme of the ALICE Collaboration. From the invariant mass resolution of the Υ resonance we

136

have defined the minimum requirements for an alignment program using physics tracks. We have developed an alignment program for the ALICE forward MUON spectrometer based on the Millepede algorithm. For this we have adapted the original Millepede fortran program into the AliMillepede class included in the general ALICE C++ software. A first test of the alignment program has been performed through full simulations in a zero magnetic field scenario. The alignment resolutions obtained are well below our requirements which confirms that we have a good alignment approach to fulfil our physics programme.

Fig. 14.14: Mean (left panels) and r.m.s (right panels) of the $\delta_x^{\mathrm{m}} - \delta_x^r$ (top), $\delta_y^{\mathrm{m}} - \delta_y^r$ (centre), and $\delta_\phi^{\mathrm{m}} - \delta_x^\phi$ (bottom) distributions as a function of the number of tracks (N_{tracks}) used by the alignment program

Further studies and developments are however still needed. In particular, in order to avoid all possible correlated displacements, further studies including global or external constraint are needed. The application of the alignment program to non-zero field data should be explored further. We also need to carry systematic analyses of the impact of misalignments on the other observables of our physics programme. Furthermore, the performance of our alignment program is currently being checked using data sets closer to what could be expected at the beginning of the LHC running. It should also be checked against different initial misalignment scenarios in order to define a valid application range. Finally, and for completeness, our alignment program should be extended to the other degrees of freedom which have so far been neglected.

Acknowledgements

References

[1] ALICE Collaboration, CERN/LHCC 99-22 (1999).

[2] ALICE Collaboration, CERN/LHCC 2000-046 (2000).

[3] R. Tieulent *et al.*, ALICE-INT-2005-009 (2005).

[4] P. Pillot, J.-Y. Grossiord, V. Kakoyan and R. Tieulent, ALICE-INT-2005-020 (2005).

[5] ALICE Collaboration, CERN/LHCC 2005-030; *J. Phys. G: Nucl. Part. Phys.* **32** (2006) 1295–2040.

[6] T. Matsui and H. Satz, *Phys. Lett. B* **178** (1986) 416.

[7] R. L. Thews, M. Schroedter and J. Rafelski, *Phys. Rev. C* **63** (2001) 054905.

[8] Z. Consea del Valle, for the ALICE Collaboration, [arXiv:nucl-ex/0609027].

[9] R. Grosso, *The ALICE alignment framework*, these proceedings.

[10] E. Dumonteil, PhD Thesis, Université de Caen (2004).

[11] V. Blobel and C. Kleinwort, [arXiv:hep-ex/0208021].

[12] V. Blobel, *Alignment algorithms*, these proceedings.

[13] The code and documentation of the Millepede program are available at http://www.desy.de/~blobel/wwwmille.html.

[14] ALICE Collaboration, ALICE-INT-2003-038 (2003).

[15] The ALICE Off-line Project policy is available at http://aliceinfo.cern.ch/Offline/ and their coding conventions are given at http://aliceinfo.cern.ch/Offline/AliRoot/Coding-Conventions.html .

[16] The AliMillepede class can be found here http://aliceinfo.cern.ch/alicvs/viewvc/MUON/AliMillepede.cxx?view=log .

[17] S. Viret, C. Parkes and D. Petrie, LHCb-2005-101 (2005); The code is available at: `http://isscvs.cern.ch/cgi-bin/cvsweb.cgi/Alignment/AlignmentTools/src/?cvsroot=lhcb`.